Dalton Transactions

ROYAL SOCIETY OF CHEMISTRY

PAPER

View Article Online
View Journal | View Issue

Cite this: *Dalton Trans.*, 2024, **53**, 13409

Two nickel-added poly(polyoxometalate)s built of Keggin-type $\{Ni_6PW_9\}$ and Anderson-type NiW_6O_{24} *via* WO_4/Sb_2O bridges and Ni–O–W linkages with efficient hydrogen evolution activity†

Peng-Yun Zhang, Chen Lian, Zhen-Wen Wang, Juan Chen, Hongjin Lv * and Guo-Yu Yang *

Received 29th March 2024,
Accepted 24th July 2024

DOI: 10.1039/d4dt00928b

rsc.li/dalton

Two Ni-added poly(polyoxometalate)s built of Keggin-type $\{Ni_6PW_9\}$ and Anderson-type NiW_6O_{24} units *via* WO_4/Sb_2O bridges and Ni–O–W linkages, $Na_4H_8[Ni(enMe)_2][(Sb_2O)_2(NiW_6O_{24})\{Ni_{12}O_2(OH)_4(enMe)_4(H_2O)_3(WO_4)_2(B\text{-}\alpha\text{-}PW_9O_{34})_2\}_2]\cdot 39H_2O$ (**1**) and $H_9[Ni(en)_2(H_2O)][Ni_{0.5}(en)_2(H_2O)][Ni(enMe)_2(H_2O)][(Sb_2O)_2(NiW_6O_{24})\{Ni_{12}O_2(OH)_4(en)_2(enMe)_2(H_2O)_3(WO_4)_2\}\text{-}\{Ni_{12}O_2(OH)_4(en)_4(H_2O)_3(WO_4)_2\}(B\text{-}\alpha\text{-}PW_9O_{34})_4]\cdot 45H_2O$ (**2**), have been hydrothermally synthesized and characterized, in which the $\{Ni_{12}(WO_4)_2(PW_9)_2\}$ subunit was obtained by the synergistic directing effect of 2 lacunary PW_9O_{34} (PW_9) fragments and further linked by a central Anderson-type $(Sb_2O)_2(NiW_6O_{24})$ bridge. Both compounds represent the first example of Ni-added polyoxometalates (POMs) simultaneously based on Keggin-type and Anderson-type POM components. Photocatalytic studies revealed that **2** can work as an efficient heterogeneous catalyst towards a light-driven H_2 evolution reaction, achieving a hydrogen evolution rate of as high as 19 214 μmol g^{-1} h^{-1} (TON = 1500), which is superior to most of the reported POM-based heterogeneous catalysts.

Introduction

To alleviate the energy crisis and environmental pollution, green and high-energy density hydrogen (H_2) will be an important energy source for future development.[1] Solar-driven water splitting has been considered a promising way to produce H_2. In particular, efforts should be concentrated on the pursuit of efficient, environmentally friendly, and cost-effective catalysts capable of splitting water into H_2. In addition to a number of nanomaterial-based photocatalysts,[2,3] an emerging type of POM-based hydrogen-evolving catalyst has been attracting tremendous attention in recent years.[4,5] POMs are typical anionic metal–oxygen clusters built of MO_x (M = Mo, W, V, Nb, Ta, *etc.*) polyhedra with diverse architectures and promising applications in catalysis, biomedicine, materials science, *etc.*[6–15] Lacunary POMs can be used as structural directing agents to induce the aggregation of transition metal (TM) ions to form TM-added POMs (TMAPs).[16–18] The introduction of TM ions imparts the TMAPs extensive tunability in structural diversity, electronic structure, and multi-electron/proton-transfer redox properties, thus benefiting photocatalytic water reduction.[19–23] Therefore, the fabrication of gigantic high-nuclearity TMAPs, such as Ni_{25}-,[24] Cu_{20}-,[25] Fe_{48}-,[26] Co_{21}-,[27] and Zr_{24}-[28] added POMs, has been continuously explored as an attractive research hotspot for several decades. Our research group has been focusing on making novel high-nuclearity Ni-added POMs (NiAPs) by the reaction of lacunary POM fragments with Ni^{2+} ions under hydrothermal conditions and achieving a series of NiAPs built by using $\{Ni_6PW_9\}$ as structural building units (SBUs).[29,30] One representative example is the 20-Ni-added POM,[31] in which the terminal and bridging O atoms of $\{Ni_4PW_6\}$ and W_4O_{16} groups substitute the water molecules and hydroxyl groups of $\{Ni_6PW_9\}$ units to build a large NiAP. Hence, the utilization of hexanuclear Ni-oxo cluster-based $\{Ni_6PW_9\}$ units as SBUs may represent a promising synthetic strategy for efficiently making high-nuclearity NiAPs.

Along with the interest in exploring high-nuclearity TM-oxo clusters, intense attention has also been focused on the combination of diverse types of POMs with different geometries and compositions to construct TMAP clusters.[32] The design and synthesis of mixed-type POM SBUs in one molecular structure not only enriches the structural diversity of POM chemistry, but also results in distinctive physicochemical properties.[33–35]

MOE Key Laboratory of Cluster Science, School of Chemistry and Chemical Engineering, Beijing Institute of Technology, Beijing 102488, China.
E-mail: ygy@bit.edu.cn, hlv@bit.edu.cn

†Electronic supplementary information (ESI) available. CCDC 2240812 and 2240815. For ESI and crystallographic data in CIF or other electronic format see DOI: https://doi.org/10.1039/d4dt00928b

Although the past several decades witnessed the prosperity and development of TMAPs with novel configurations, most of them are assembled by only one type of POM fragment.[36–40] TMAPs containing mixed-type POM fragments with diverse electronic configurations and molecular sizes have rarely been reported, and most of the TMAPs have been made from lacunary Keggin and Dawson-type POM units, such as $[Mn_6(PW_6O_{26})(\alpha\text{-}P_2W_{15}O_{56})_2(H_2O)_2]^{23-}$,[41] $[Zr_3(\mu_2\text{-}OH)_2(\mu_2\text{-}O)(A\text{-}\alpha\text{-}GeW_9O_{34})(1,4,9\text{-}\alpha\text{-}P_2W_{15}O_{56})]^{14-}$,[42] *etc*. In contrast, the coexistence of Keggin and Anderson-type POMs in one TMAP framework is extremely uncommon. Additionally, the so-called Anderson-type fragment of one representative compound $[As_6Fe_7Mo_{22}O_{98}]^{25-}$ is different from the classic Anderson-type XM_6O_{24} unit.[43] Therefore, it is of high significance but a challenging goal to make structurally-new TMAPs with mixed Keggin- and Anderson-type POM fragments.

Herein, we report two Ni-added POMs, $Na_4H_8[Ni(enMe)_2][(Sb_2O)_2(NiW_6O_{24})\{Ni_{12}O_2(OH)_4(enMe)_4(H_2O)_3(WO_4)_2(B\text{-}\alpha\text{-}PW_9O_{34})_2\}_2]\cdot 39H_2O$ (**1**) and $H_9[Ni(en)_2(H_2O)][Ni_{0.5}(en)_2(H_2O)][Ni(enMe)_2(H_2O)][(Sb_2O)_2(NiW_6O_{24})\{Ni_{12}O_2(OH)_4(en)_2(enMe)_2(H_2O)_3(WO_4)_2\}\{Ni_{12}O_2(OH)_4(en)_4(H_2O)_3(WO_4)_2\}(B\text{-}\alpha\text{-}PW_9O_{34})_4]\cdot 45H_2O$ (**2**). Both clusters can be simplified as four Keggin-type $\{Ni_6PW_9\}$ units linked by one central Anderson-type NiW_6O_{24} subunit and further stabilized by WO_4/Sb_2O bridges and Ni–O–W linkages. **1** is a one-dimensional (1D) chain linked by $[Ni(enMe)_2]^{2+}$ complexes, while **2** is a discrete cluster. In addition, **1** and **2** can work as multi-electron-transfer catalysts to drive photocatalytic H_2 evolution reactions. **2** exhibited high efficiency in heterogeneous photocatalytic H_2 production with the highest H_2 evolution rate of up to 19 214 μmol g^{-1} h^{-1} (TON = 1500).

Results and discussion

Structural description

Single crystal X-ray diffraction shows that **1** (Fig. 1a and b, S1†) crystallizes in the triclinic space group $P\bar{1}$ (Table 1) and consists of a $[(Sb_2O)_2(NiW_6O_{24})\{Ni_{12}O_2(OH)_4(enMe)_4(H_2O)_3(WO_4)_2(PW_9O_{34})_2\}_2]^{14-}$ polyoxoanion (**1a**), one bridging complex $[Ni(enMe)_2]^{2+}$, 4 Na^+, 8 protons, and 39 lattice water molecules. The bond lengths of Ni–O and Ni–N range from 1.99 to 2.26 Å, and the valence states of Ni atoms are all +2 according to the bond valence sum (BVS) calculations (Table S1†). The hourglass-like polyoxoanion **1a** comprises two different $\{Ni_6\}$ clusters, namely $[Ni_6O_6(OH)_3(enMe)_2(H_2O)_2]^{3-}$ (**Ni_6-1**, Fig. S2a†) and $[Ni_6O_9(OH)(enMe)_2(H_2O)]^{7-}$ (**Ni_6-2**, Fig. S2b†), added Keggin subunits, one central Anderson $[NiW_6O_{24}]^{10-}$ unit, and two kinds of linkers WO_4 and Sb_2O. The **Ni_6-1** subunit not only connects with 2 WO_4 units, but also has 2 terminal water molecules which are further substituted by 2 terminal O atoms (O44, O48) of the $[NiW_6O_{24}]^{10-}$ unit (Fig. 1c). In contrast, the **Ni_6-2** subunit not only links with 2 WO_4 units, but also has 3 terminal water molecules which are substituted by 2 terminal O(35, 39) atoms and 1 bridging O26 atom of the $[NiW_6O_{24}]^{10-}$ unit (Fig. 1d). Additionally, 2 μ_3-O(27, 25) atoms of **Ni_6-2** form a linkage with 2 μ_3-O(41, 45) atoms of the $[NiW_6O_{24}]^{10-}$ unit through a Sb_2O moiety

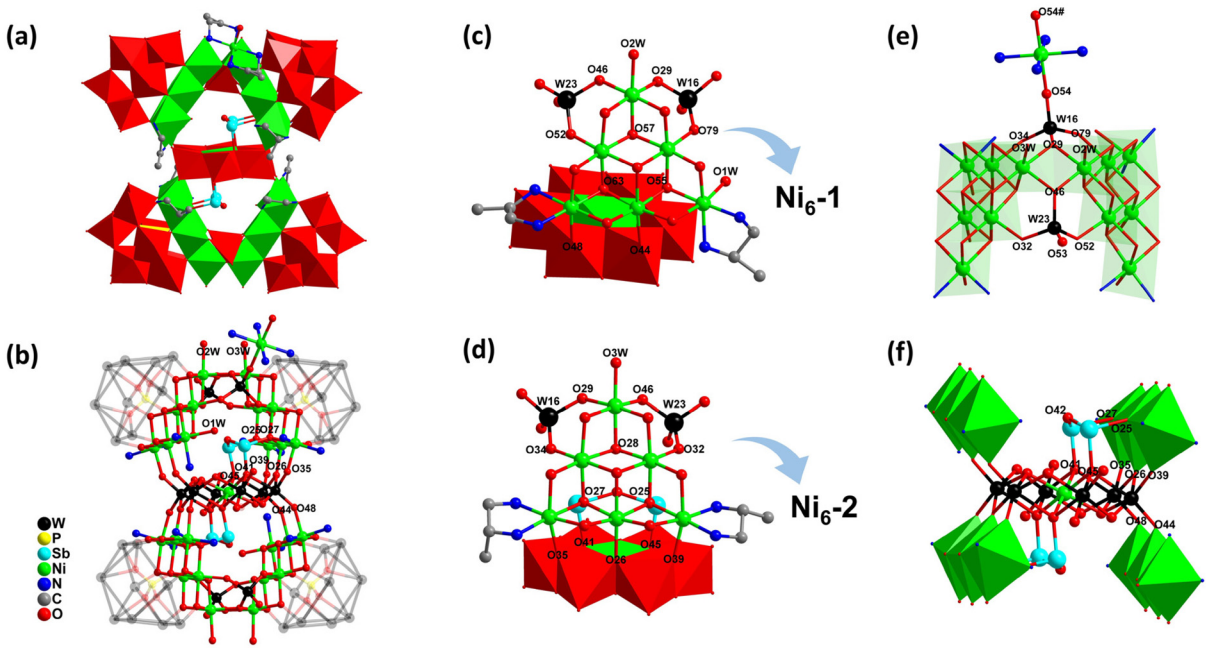

Fig. 1 (a) and (b) The view of **1**. (c) The coordination environment of the **Ni_6-1** unit. (d) The coordination environment of the **Ni_6-2** unit. (e) The formation of **1b** under the stabilizing effect of WO_4 units. Symmetry code: #: 2 – *x*, 1 – *y*, –*z*. (f) The connection mode of Anderson-type POM binding with the Ni^{2+} ions and Sb^{3+} ions. Color labels for polyhedra: WO_6 or WO_4, red; PO_4, yellow; NiO_6 or NiO_4N_2, green. Note: all the H atoms and some C atoms are omitted for clarity.

Table 1 Crystallographic data and structure refinements for **1** and **2**

	1	2
CCDC	2240812	2240815
Formula	$C_{30}H_{206}N_{20}Na_4Ni_{26}O_{235}P_4Sb_4W_{46}$	$C_{32}H_{245}N_{28}Ni_{27.5}O_{244}P_4Sb_4W_{46}$
M_r	15 294.54	15 610.05
Crystal system	Triclinic	Monoclinic
Space group	$P\bar{1}$	Cc
a/Å	14.1447(7)	36.8164(10)
b/Å	19.4035(9)	29.8064(8)
c/Å	22.8651(10)	25.4292(7)
α/°	90.1970(10)	90
β/°	106.1290(10)	105.4530(10)
γ/°	98.5440(10)	90
V/Å^3	5955.0(5)	26 896.3(13)
Z	1	4
D_c/g cm^{-3}	4.265	3.855
μ/mm^{-1}	24.711	21.987
F(000)	6846.0	28 092.0
GOF on F^2	1.034	1.037
Final R indexes $[I \geq 2\sigma(I)]^a$	R_1 = 0.0456, wR_2 = 0.0951	R_1 = 0.0463, wR_2 = 0.0978
Final R indexes [all data]	R_1 = 0.0624, wR_2 = 0.1009	R_1 = 0.0638, wR_2 = 0.1024

^{a} $R = \sum||F_o| - |F_c||/\sum|F_o|$, $wR_2 = [\sum w(F_o^2 - F_c^2)^2/\sum w(F_o^2)^2]^{1/2}$.

(Fig. 1d). The BVS results of O55, O63, and O57 in **Ni_6-1** are 1.08, 1.11, and 1.12 (Table S1†), respectively, indicating the monoprotonated nature of these μ_3-O atoms. However, the BVS results of 3 homologous O(25, 27, 28) atoms in **Ni_6-2** are 2.01, 2.02, and 1.17 (Table S1†), respectively, illustrating that only O28 is monoprotonated. Different from μ_3-O28, the μ_4-O25 and μ_4-O27 atoms in **Ni_6-2** not only act as bridges for 3 Ni^{2+} ions but also connect with an Sb^{3+} ion.

The **Ni_6-1** and **Ni_6-2** subunits are integrated to form a $[Ni_{12}O_7(OH)_4(enMe)_4(H_2O)_3(WO_4)_2]^{2+}$ cluster (**1b**) through 2 Ni^{2+} ions located at the vertices of the {**Ni_6**} clusters in an edge-sharing manner (O29 and O46 are shared), which were further stabilized by 2 WO_4 groups (Fig. 1e). The connection mode of **1b** is different from the previously reported Ni_{12}-based POMs formed by 2 $\{Ni_6SiW_9\}$ units *via* Ni–O–W bonds.[44] Each WO_4 group substitutes 2 terminal coordination water molecules (O34 and O79 for W16; O32 and O52 for W23) of 2 Ni^{2+} ions in 2 $\{Ni_6\}$ clusters, respectively, and further connects with the edge-sharing Ni^{2+} ions (Fig. 1e). Different from the W23 center, the W16 center of the WO_4 group is further supported by a bridging complex $[Ni(enMe)_2]^{2+}$ *via* the O54 atom, which links adjacent polyoxoanions to form a AAA 1D chain (Fig. 2). The formation of the 1D chain through Ni-amine complexes that are supported on the WO_4 ligand is rarely reported. In most instances, the complexes are supported on the WO_6 of XW_9 (X = P, Si, Ge) units.[45] Significantly, the 57° angle between **Ni_6-1** and **Ni_6-2** units results in *ca.* 8.1 Å between the Ni^{2+} ions on both sides of the opening position (Fig. S3a†), which matches approximately with the diameter of the Anderson-type cluster (*ca.* 7.6 Å, Fig. S3b†), providing a possibility of confined growth.

The central Ni-containing Anderson-type unit consists of 6 WO_6 octahedra linked in edge-sharing mode, which could be

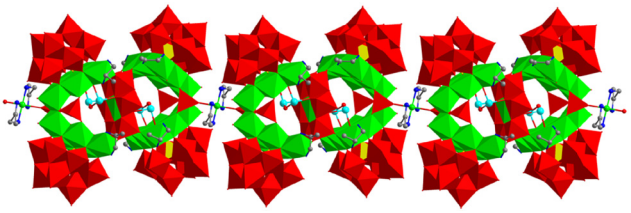

Fig. 2 The AAA 1D chains formed by adjacent polyoxoanion clusters **1a** and $[Ni(enMe)_2]^{2+}$ linkers. Color labels for polyhedra: WO_6 or WO_4, red; PO_4, yellow; NiO_6 or NiO_4N_2, green. Note: all the H atoms are omitted for clarity.

derived from the transformation of $[PW_9O_{34}]^{9-}$ units. To date, the Anderson-type precursors have been commonly functionalized by triol organic ligands or tri-dentate inorganic groups.[46–49] However, in this polyoxoanion, the terminal and bridging oxygen atoms of the Anderson $[NiW_6O_{24}]^{10-}$ unit substitute 2 water molecules of **Ni_6-1** units and 3 water molecules of **Ni_6-2** units on two sides through 10 Ni–O–W bonds (Fig. 1f). Moreover, as previously mentioned, 2 μ_3-O(41,45) atoms of the $[NiW_6O_{24}]^{10-}$ unit connect with 2 μ_3-O(27,25) atoms of **Ni_6-2** through a Sb_2O moiety on both sides (Fig. 1f). In POM chemistry, Sb atoms are usually present as heteroatoms in precursor species.[50,51] However, they function as bridging entities within the framework of **1** in this work.

By following the synthetic strategy of **1**, the introduction of mixed organic amines (en and enMe) led to the formation of an isolated cluster $H_9[Ni(en)_2(H_2O)][Ni_{0.5}(en)_2(H_2O)][Ni(enMe)_2(H_2O)][(Sb_2O)_2(NiW_6O_{24})\{Ni_{12}O_2(OH)_4(en)_2(enMe)_2(H_2O)_3(WO_4)_2\}\{Ni_{12}O_2(OH)_4(en)_4(H_2O)_3(WO_4)_2\}(B\text{-}\alpha\text{-}PW_9O_{34})_4]\cdot 45H_2O$ (**2**, Fig. 3a and S4†). **2** crystallized in the monoclinic space group *Cc* (Table 1) and can be viewed as the assembly of a polyoxoanion cluster $[(Sb_2O)_2(NiW_6O_{24})\{Ni_{12}O_2(OH)_4(en)_2(enMe)_2(H_2O)_3(WO_4)_2\}\text{-}\{Ni_{12}O_2(OH)_4(en)_4(H_2O)_3(WO_4)_2\}(B\text{-}\alpha\text{-}PW_9O_{34})_4]^{14-}$ (**2a**) similar to **1a** except for the different coordination

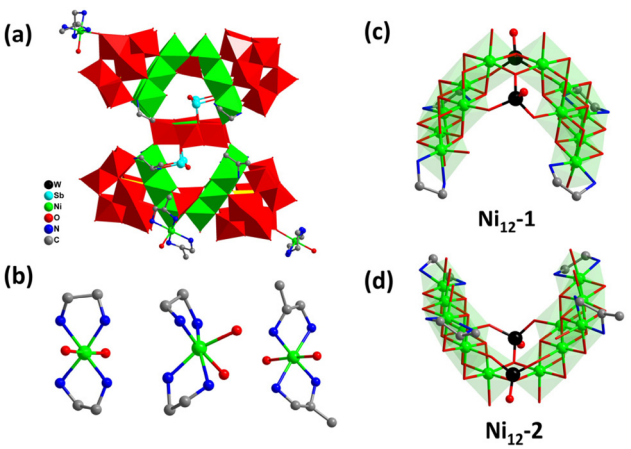

Fig. 3 (a) Compound **2**. (b) Three different counter cations of **2**. (c) The **Ni_{12}-1** cluster. (d) The **Ni_{12}-2** cluster. Color labels for polyhedra: WO_6 or WO_4, red; PO_4, yellow; NiO_6 or NiO_4N_2, green. Note: all the H atoms are omitted for clarity.

amine molecules to Ni^{2+} ions, three counter cations of $[Ni(en)_2(H_2O)]^{2+}$, $[Ni_{0.5}(en)_2(H_2O)]^{+}$, and $[Ni\text{-}(enMe)_2(H_2O)]^{2+}$ complexes (Fig. 3b), 9 protons, and 45 lattice water molecules. **2a** is built of one $[(Sb_2O)_2NiW_6O_{24}]^{2-}$ unit integrating two different $\mathbf{Ni_{12}}$-clusters, $[Ni_{12}O_7(OH)_4(en)_4(H_2O)_3(WO_4)_2]^{2+}$ ($\mathbf{Ni_{12}}$**-1**, Fig. 3c) and $[Ni_{12}O_7(OH)_4(en)_2(enMe)_2(H_2O)_3(WO_4)_2]^{2+}$ ($\mathbf{Ni_{12}}$**-2**, Fig. 3d), added POM moieties. The difference between such two $\mathbf{Ni_{12}}$ clusters is caused by the different types and orientations of organic amines. Considering the acentric *Cc* space group of **2**, a second-harmonic-generation (SHG) test of the sieved crystals was conducted by employing a Q-switched Nd:YAG laser (1064 nm). As illustrated in Fig. S5,† sample **2** manifested an SHG response approximately 0.6 times that of KDP, revealing its potential utilization as a nonlinear optical material.[52]

Photocatalytic properties

Inspired by the properties of TMAPs synthesized using transition metals as active sites and POM ligands as electron sponges, we expected that **1** and **2** should be potential catalysts for the H_2 evolution reaction. To evaluate their visible-light-driven catalytic activity, a well-established three-component catalytic system was employed.[5,53] The mixture containing **1** or **2** as catalysts, 0.3 mM $[Ir(coumarin)_2(dtbbpy)]^{+}$ as a photosensitizer, 0.2 M triethanolamine (TEOA) as a sacrificial electron donor, and 2.5 M H_2O as a proton source in DMF/CH_3CN (6 ml, v/v, 3/1) was degassed with Ar/CH_4 (v/v, 4/1) and irradiated under 10 W white light (λ = 400–800 nm) at 25 °C. The evolved H_2 was detected by gas chromatography and quantified based on the internal CH_4 standard.

Under otherwise identical conditions, the amount of H_2 generated reached 55 μmol and 69 μmol after 5 hours of irradiation while using 1 mg of **1** and **2** as catalysts, respectively (Fig. S6†). Therefore, **2** was used for the following studies unless otherwise noted. Upon illumination of white LED light, the continuous generation of H_2 gas was detected over time. As shown in Fig. 4a, varying the catalyst dosage from 0.5 mg to 4 mg resulted in an increasing H_2 evolution from 48 μmol to 119 μmol, respectively. However, the corresponding H_2 evolution rate decreased from 19 214 μmol g^{-1} h^{-1} to 5959 μmol g^{-1} h^{-1} and the calculated turnover number (TON) also decreased from 1500 to 465 (Fig. 4b), which is probably attributed to the strong light scattering effect of the heterogeneous photocatalytic system at the high amount of catalyst, thereby leading to a decreased incident photon absorption. The present H_2 evolution rate of 19 214 μmol g^{-1} h^{-1} (TON = 1500) revealed the outstanding catalytic activity of **2** which was superior to that of most heterogeneous POM-based catalysts (Table S2†).

Various control experiments were further conducted to better understand the catalytic system. Running the reaction in the dark environment resulted in no production of H_2, indicating the light-driven nature of the catalytic reaction (Fig. 4c). Moreover, the absence of $[Ir(coumarin)_2(dtbbpy)]^{+}$, TEOA, or catalyst **2** in these blank control tests yielded no or negligible

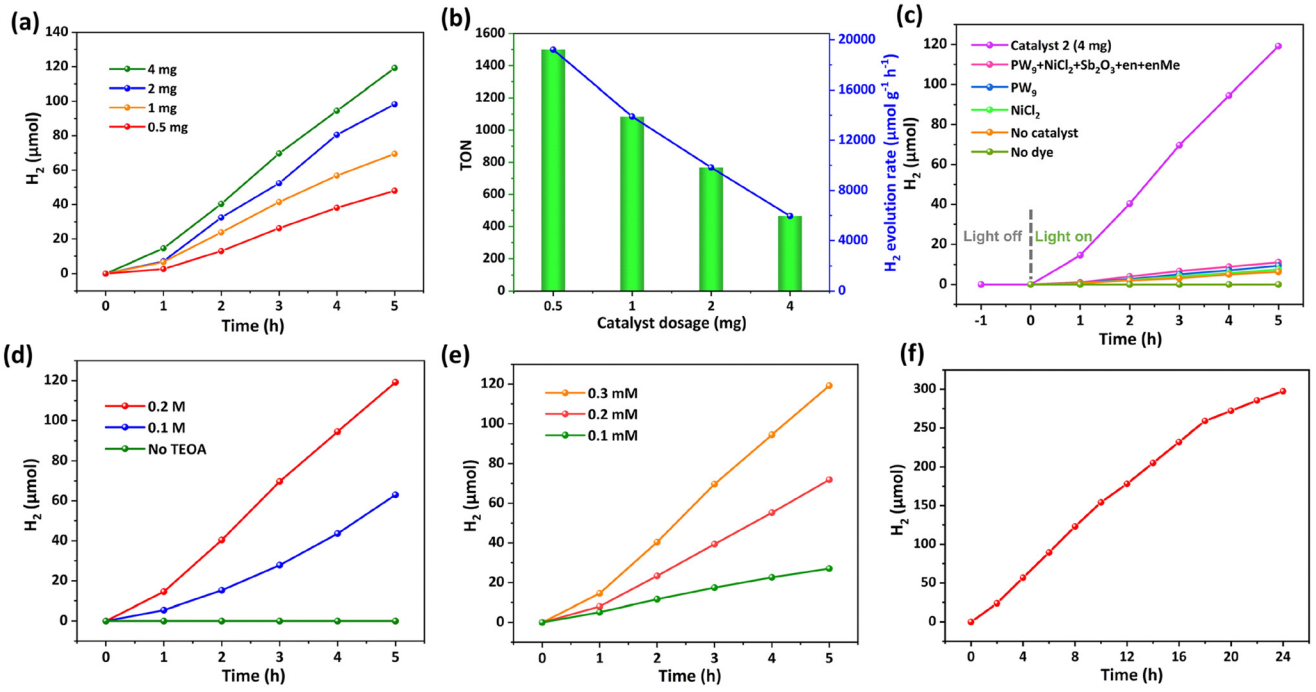

Fig. 4 (a) Time-dependent H_2 evolution activity and (b) the TON and H_2 evolution rate with different amounts of catalyst **2** (0.5–4 mg). Conditions: white light (10 W, 400–800 nm), 0.3 mM $[Ir(coumarin)_2(dtbbpy)]^{+}$, 0.2 M TEOA, 2.5 M H_2O, 6 mL DMF/CH_3CN (v/v, 3/1) degassed with Ar/CH_4 (v/v, 4/1). (c) Blank control tests without illumination, dye, or catalyst, and parallel tests with different catalysts for H_2 evolution. (d) Control tests for H_2 evolution with different TEOA concentrations (0–0.2 M), (e) different $[Ir(coumarin)_2(dtbbpy)]^{+}$ concentrations (0.1–0.3 mM) and (f) the long-term catalytic process under illumination for 24 h.

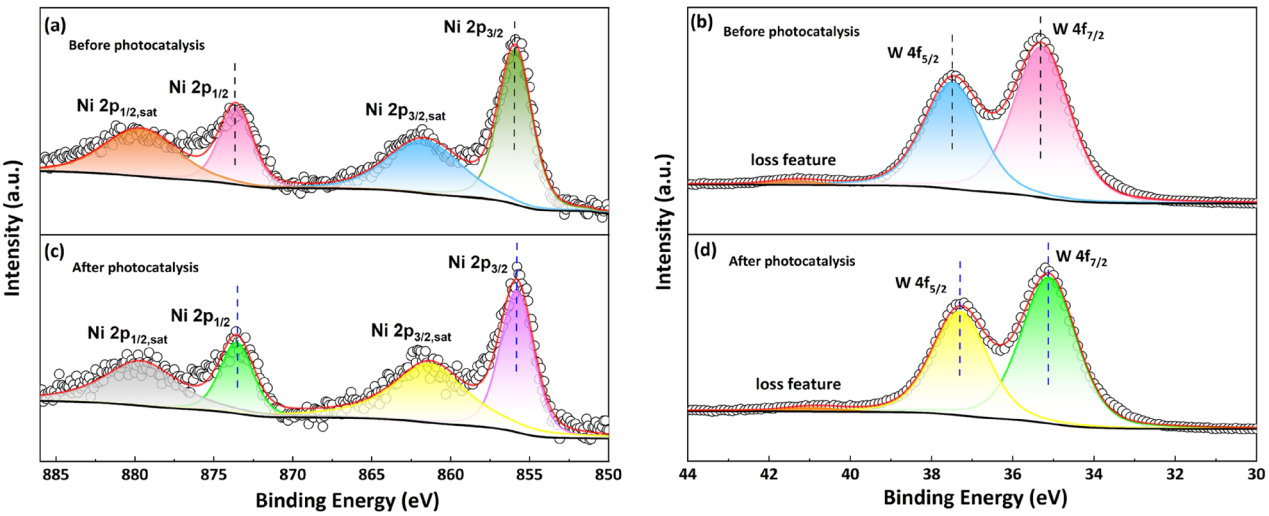

Fig. 5 The XPS spectra of fresh compound **2** before catalysis: (a) Ni 2p and (b) W 4f; and the spectra of recovered catalyst **2** after catalysis: (c) Ni 2p and (d) W 4f.

H_2, respectively (Fig. 4c and d). Such a phenomenon proved that any one of these three components is indispensable for efficient photocatalysis. Further parallel tests by replacing catalyst **2** with the molar equivalents of PW_9, $NiCl_2$ or mixed reactants including PW_9, $NiCl_2$, Sb_2O_3, en and enMe also produced a small amount of H_2 (Fig. 4c). In addition, the increment of both TEOA concentration from 0 to 0.2 M (Fig. 4d) and $[Ir(coumarin)_2\text{-}(dtbbpy)]^+$ concentration from 0.1 mM to 0.3 mM (Fig. 4e) positively contributed to the production of H_2.

Then, we studied the stability of catalyst **2** under simulated photo-catalytic conditions by immersing the fresh samples into different solutions including acidic HCl aqueous solution (pH = 3), alkaline NaOH aqueous solution (pH = 13), and organic solvents ($DMF : CH_3CN$ = v/v, 3 : 1) for 24 h. The IR spectra and PXRD patterns of the soaked samples are consistent with those of the freshly synthesized samples, demonstrating the chemical stability of catalyst **2** in acids, bases, and organic solvents (Fig. S7†). The long-term stability of catalyst **2** was further evaluated under turnover conditions by performing the catalytic reaction for 24 h in the presence of 1 mg of catalyst **2**. The H_2 evolution yield can achieve 297 μmol with an H_2 production rate of 12 390 μmol g^{-1} h^{-1} at a 24 hour time scale, proving the robustness of the light-driven catalytic system (Fig. 4f). The easy recovery and reusability of catalysts are important attributes of heterogeneous catalytic systems. To better evaluate the performance of catalyst **2**, three successive recycling tests were carried out using 2 mg of catalyst **2** (Fig. S8†). After completing one catalytic test, the catalyst was isolated by centrifugation, washed with CH_3CN, and reused in a fresh reaction solution for subsequent cycles. It is noted that the slight decrease of H_2 yield after each cycle could be attributed to the loss of catalyst during isolation treatment. The IR spectra and PXRD patterns before and after catalysis remained largely unchanged, illustrating the stability of catalyst **2** (Fig. S9†).

Generally, POM-based catalysts can function as multi-electron-storing/transferring mediators in the photocatalytic process, accompanied by the reduction of Mo^{6+} to Mo^{5+} or W^{6+} to W^{5+} to form heteropoly blue species.[54] In this work, since no obvious color change of the catalyst was observed by the naked eye, we speculated that the stored electrons in catalyst **2** can be quickly utilized for H_2 generation. To deeply elucidate this process, X-ray photoelectron spectroscopy (XPS) measurements were further performed to reveal the chemical environment and oxidation changes of catalyst **2** before and after photocatalysis. The full survey XPS spectra show well-matched elemental signals of catalyst **2** before and after catalysis, implying good catalyst stability (Fig. S10†). The Ni $2p_{3/2}$ and Ni $2p_{1/2}$ signals of the fresh catalyst **2** before catalysis were observed at 855.9 eV and 873.6 eV (Fig. 5a), respectively, indicating a +2 state of Ni ions. The oxidation state of W atoms was assigned as +6 as revealed by binding energies of W $4f_{7/2}$ and W $4f_{5/2}$ at 35.3 eV and 37.5 eV (Fig. 5b). In contrast, slight negative shifts of 0.1 eV and 0.2 eV were observed for Ni 2p and W 4f signals after photocatalysis (Fig. 5c and d), respectively, which could be caused by partial reduction of catalyst **2** during catalysis.[55] It is worth mentioning that the reduction of W is not as obvious as that observed in a reported polyoxomolybdate-based catalytic system,[49] where the reduction of Mo^{6+} to Mo^{5+} was detected in the XPS spectra after catalysis. Such discrepancy should be ascribed to the oxidation potential difference between Mo^{6+}/Mo^{5+} and W^{6+}/W^{5+},[56] and Mo^{5+} can stably exist under ambient conditions while W^{5+} tends to be oxidized back to W^{6+} upon exposure to air.

Conclusions

In summary, we have synthesized two unprecedented mixed-type Keggin and Anderson POM-based NiAPs, $[(Sb_2O)_2(NiW_6O_{24})$-

$\{Ni_{12}O_2(OH)_4(enMe)_4(H_2O)_3(WO_4)_2(PW_9O_{34})_2\}_2]^{14-}$ and $[(Sb_2O)_2(NiW_6O_{24})\{Ni_{12}O_2(OH)_4(en)_2(enMe)_2(H_2O)_3(WO_4)_2\}\{Ni_{12}O_2(OH)_4(en)_4(H_2O)_3(WO_4)_2\}(PW_9O_{34})_4]^{14-}$, under hydrothermal conditions. The resulting two polyoxoanions could be structurally viewed as one central $\{(Sb_2O)_2(NiW_6O_{24})\}$ fragment linking two $\{Ni_{12}(WO_4)_2(PW_9)_2\}$ subunits through Sb_2O moieties and Ni–O–W bonds. In addition, **1** is the first 1D chain linked by $[Ni(enMe)_2]^{2+}$ complexes and 25-Ni incorporated POMs. Upon light irradiation, **2** exhibited effective H_2 evolution activity in a three-component photocatalytic system, which is superior to most of the reported POM-based heterogeneous catalysts. The present work not only enriches the structural diversity of POM chemistry, but also encourages the future exploration of POM-based catalysts for solar energy conversion.

Experimental

Synthesis of 1

A mixture of $NiCl_2{\cdot}6H_2O$ (0.802 g, 3.374 mmol), $Na_9[A\text{-}\alpha\text{-}PW_9O_{34}]{\cdot}7H_2O$ (1.882 g, 0.734 mmol), K_2CO_3 (0.205 g, 1.483 mmol), $NH_4B_5O_8{\cdot}4H_2O$ (0.503 g, 1.848 mmol) and Sb_2O_3 (0.125 g, 0.429 mmol) was dissolved in 15 ml distilled water under continuous stirring. Then 0.20 ml of 1,2-enMe (1,2-diaminopropane) was dropwise added to the cloudy solution and the pH was adjusted to 6.8 with 4 M HCl solution. After two hours of stirring, the solution was sealed and placed in an oven at 170 °C for 10 days. After cooling down to room temperature naturally, green crystals were obtained. Yield: 41% based on $Na_9[A\text{-}\alpha\text{-}PW_9O_{34}]{\cdot}7H_2O$. Elemental analysis calc. for **1** (%): C 2.36, H 1.36, N 1.83, Ni 9.98, Sb 3.18, W 55.30; found: C 2.47, H 1.54, N 1.98, Ni 10.12, Sb 3.31, W 55.49. IR (KBr, cm^{-1}, Fig. S11a†): 3446 (vs), 2925 (w), 1622 (s), 1464 (w), 1403 (w), 1046 (s), 949 (s), 845 (w), 793 (m) and 722 (s). As shown in Fig. S12a,† the experimental powder X-ray diffraction (PXRD) of **1** matches well with the simulated results derived from the single crystal diffraction data. The thermogravimetric analysis (TGA) was conducted from 25 to 700 °C (Fig. S13a†), and a weight loss of 14.27% was detected for **1** (see the ESI† for details). The band gap value of 3.41 eV for **1** demonstrated the properties of a semiconductor (see the ESI for details, Fig. S14a†).

Synthesis of 2

The synthetic process of **2** is similar to that of **1** except for the employment of mixed organic amines en (ethylenediamine, 0.10 ml) and 1,2-enMe (0.10 ml) as a substitute for 1,2-enMe (0.20 ml) and reducing the reaction time from 10 days to 5 days. Green crystals were obtained in a yield of 39% based on $Na_9[A\text{-}\alpha\text{-}PW_9O_{34}]{\cdot}7\ H_2O$. Elemental analysis calc. for **2** (%): C 2.46, H 1.58, N 2.51, Ni 10.34, Sb 3.12, W 54.18; found: C 2.59, H 1.64, N 2.67, Ni 10.41, Sb 3.27, W 55.36. IR (KBr, cm^{-1}, Fig. S11b†): 3450 (vs), 2950 (w), 1636 (s), 1458 (w), 1391 (w), 1040 (s), 943 (s), 835 (m), 792 (m) and 725 (s). The experimental PXRD of **2** coincides well with the simulated patterns from the single crystal diffraction data (Fig. S12b†). The TGA curve showed a weight loss of 12.84% for compound **2** from 25 to 700 °C (see the ESI for details, Fig. S13b†). The band gap value of **2** was 3.32 eV, revealing that **2** is a potential semiconductor material (see the ESI for details, Fig. S14b†).

Author contributions

Peng-Yun Zhang: methodology, investigation, data curation, formal analysis, and writing – original draft. Chen Lian: writing – review & editing. Zhen-Wen Wang: data curation. Juan Chen: investigation. Hongjin Lv: writing – review & editing. Guo-Yu Yang: validation, writing – review & editing, and funding acquisition.

Data availability

The data supporting this article have been included as part of the ESI.† Crystallographic data for compounds **1** and **2** have been deposited at the CCDC under 2240812 and 2240815.

Electronic supplementary information (ESI) available: experimental procedures, IR spectra, thermogravimetric analyses, optical band gaps, and supporting figures and tables. CCDC 2240812 (**1**) and 2240815 (**2**).

Conflicts of interest

There are no conflicts to declare.

Acknowledgements

The authors sincerely acknowledge the financial support from the National Natural Science Foundation of China (no. 21831001, 21571016, 91122028, and 21871025) and the National Natural Science Foundation of China for Distinguished Young Scholars (No. 20725101).

References

1 Q. Shen, C. J. Gómez-García, W. Sun, X. Lai, H. Pang and H. Ma, *Green Chem.*, 2021, **23**, 3104.
2 D. Zeng, P. Wu, W. J. Ong, B. Tang, M. Wu, H. Zheng, Y. Chen and D. L. Peng, *Appl. Catal., B*, 2018, **233**, 26.
3 S. H. Chen, W. T. Wang, Y. Hou, Y. C. Hao, Y. C. Zhao, S. Y. Wang, J. F. Meng and H. Y. Xu, *ACS Appl. Nano Mater.*, 2023, **6**, 8717.
4 N. Li, J. Liu, B. X. Dong and Y. Q. Lan, *Angew. Chem., Int. Ed.*, 2020, **59**, 20779.
5 H. J. Lv, W. W. Guo, K. F. Wu, Z. Y. Chen, J. Bacsa, D. G. Musaev, Y. V. Geletii, S. M. Lauinger, T. Q. Lian and C. L. Hill, *J. Am. Chem. Soc.*, 2014, **136**, 14015.
6 C. F. Li, K. Yamaguchi and K. Suzuki, *Angew. Chem., Int. Ed.*, 2021, **60**, 6960.

7 L. Yang, Z. Zhang, C. N. Zhang, S. Li, G. C. Liu and X. L. Wang, *Inorg. Chem. Front.*, 2022, **9**, 4824.
8 Z. M. Zhang, S. Yao, Y. G. Li, H. H. Wu, Y. H. Wang, M. Rouzières, R. Clérac, Z. M. Su and E. B. Wang, *Chem. Commun.*, 2013, **49**, 2515.
9 Z. Zhang, Y. L. Wang, H. L. Li, K. N. Sun and G. Y. Yang, *CrystEngComm*, 2019, **21**, 2641.
10 X. K. Fang and M. Luban, *Chem. Commun.*, 2011, **47**, 3066.
11 Y. L. Wu, X. X. Li, Y. J. Qi, H. Yu, L. Jin and S. T. Zheng, *Angew. Chem., Int. Ed.*, 2018, **57**, 8572.
12 W. H. Fang, W. D. Wang and G. Y. Yang, *Dalton Trans.*, 2015, **44**, 12546.
13 M. Ibrahim, Y. Xiang, B. S. Bassil, Y. Lan, A. K. Powell, P. de Oliveira, B. Keita and U. Kortz, *Inorg. Chem.*, 2013, **52**, 8399.
14 P. E. Car, M. Guttentag, K. K. Baldridge, R. Alberto and G. R. Patzke, *Green Chem.*, 2012, **14**, 1680.
15 P. Y. Zhang, Z. Zhang, X. Y. Li and G. Y. Yang, *Inorg. Chem. Commun.*, 2020, **113**, 107753.
16 S. T. Zheng, D. Q. Yuan, H. P. Jia, J. Zhang and G. Y. Yang, *Chem. Commun.*, 2007, **18**, 1858.
17 C. Lian, H. L. Li and G. Y. Yang, *Sci. China: Chem.*, 2023, **66**, 1394.
18 P. Y. Zhang, Y. Wang, L. Y. Yao and G. Y. Yang, *Inorg. Chem.*, 2022, **61**, 10410.
19 X. J. Kong, Z. Lin, Z. M. Zhang, T. Zhang and W. B. Lin, *Angew. Chem., Int. Ed.*, 2016, **55**, 6411.
20 X. B. Han, C. Qin, X. L. Wang, Y. Z. Tan, X. J. Zhao and E. B. Wang, *Appl. Catal., B*, 2017, **211**, 349.
21 Y. H. Zhu, Z. Y. Du, J. L. Wang, J. B. Yang, H. Mei and Y. Xu, *Inorg. Chem.*, 2022, **61**, 20397.
22 X. Q. Du, J. L. Zhao, J. Q. Mi, Y. Ding, P. P. Zhou, B. C. Ma, J. W. Zhao and J. Song, *Nano Energy*, 2015, **16**, 247.
23 H. L. Li, M. Zhang, C. Lian, Z. L. Lang, H. J. Lv and G. Y. Yang, *CCS Chem.*, 2021, **3**, 2095.
24 X. B. Han, Y. G. Li, Z. M. Zhang, H. Q. Tan, Y. Lu and E. B. Wang, *J. Am. Chem. Soc.*, 2015, **137**, 5486.
25 S. S. Mal and U. Kortz, *Angew. Chem., Int. Ed.*, 2005, **44**, 3777.
26 J. Goura, B. S. Bassil, J. K. Bindra, I. A. Rutkowska, P. J. Kulesza, N. S. Dalal and U. Kortz, *Chem. – Eur. J.*, 2020, **26**, 15821.
27 D. Y. Shi, C. J. Cui, C. X. Sun, J. P. Du and C. S. Liu, *New J. Chem.*, 2020, **44**, 11336.
28 L. Huang, S. S. Wang, J. W. Zhao, L. Cheng and G. Y. Yang, *J. Am. Chem. Soc.*, 2014, **136**, 7637.
29 S. T. Zheng, J. Zhang, X. X. Li, W. H. Fang and G. Y. Yang, *J. Am. Chem. Soc.*, 2010, **132**, 15102.
30 L. Huang, J. Zhang, L. Cheng and G. Y. Yang, *Chem. Commun.*, 2012, **48**, 9658.
31 S. T. Zheng, J. Zhang, J. M. Clemente-Juan, D. Q. Yuan and G. Y. Yang, *Angew. Chem., Int. Ed.*, 2009, **48**, 7176.
32 H. L. Li, C. Lian, L. J. Chen, J. W. Zhao and G. Y. Yang, *Nanoscale*, 2020, **12**, 16091.
33 D. E. S. Marcano, M. A. Moussawi, A. V. Anyushin, S. Lentink, L. V. Meervelt, L. Ivanović-Burmazović and T. N. ParacVogt, *Chem. Sci.*, 2022, **13**, 2891.
34 H. L. Li, C. Lian and G. Y. Yang, *Inorg. Chem.*, 2023, **62**, 9014.
35 M. Y. Cheng, H. Y. Wang, Y. F. Liu, J. W. Shi, M. Q. Zhou, W. X. Du, D. D. Zhang and G. P. Yang, *Chin. Chem. Lett.*, 2023, **34**, 107209.
36 X. X. Li, W. H. Fang, J. W. Zhao and G. Y. Yang, *Chem. – Eur. J.*, 2015, **21**, 2315.
37 S. T. Zheng, J. Zhang and G. Y. Yang, *Angew. Chem., Int. Ed.*, 2008, **47**, 3909.
38 X. X. Li, X. Ma, W. X. Zheng, Y. J. Qi, S. T. Zheng and G. Y. Yang, *Inorg. Chem.*, 2016, **55**, 8257.
39 H. J. Lv, Y. Chi, J. van Leusen, P. Kögerler, Z. Chen, J. Bacsa, Y. V. Geletii, W. W. Guo, T. Lian and C. L. Hill, *Chem. – Eur. J.*, 2015, **21**, 17363.
40 J. Goura, B. S. Bassil, X. Ma, A. Rajan, E. Moreno-Pineda, J. Schnack, M. Ibrahim, A. K. Powell, M. Ruben, J. P. Wang, L. Ruhlmann and U. Kortz, *Chem. – Eur. J.*, 2021, **27**, 15081.
41 M. Martin-Sabi, R. S. Winter, C. Lydon, J. M. Cameron, D. L. Long and L. Cronin, *Chem. Commun.*, 2016, **52**, 919.
42 Z. Zhang, J. W. Zhao and G. Y. Yang, *Eur. J. Inorg. Chem.*, 2017, 3244.
43 P. F. Wu, Y. P. Zhang, C. T. Feng, B. Liu, H. M. Hu and G. L. Xue, *Dalton Trans.*, 2018, **47**, 15661.
44 L. Yang, Y. Huo and J. Y. Niu, *Dalton Trans.*, 2013, **42**, 364.
45 X. X. Li, S. T. Zheng, J. Zhang, W. H. Fang, G. Y. Yang and J. M. Clemente-Juan, *Chem. – Eur. J.*, 2011, **17**, 13032.
46 Q. H. Zhuang, Z. Q. Sun, C. G. Lin, B. Qi and Y. F. Song, *Inorg. Chem. Front.*, 2023, **10**, 1695.
47 A. Macdonell, N. A. B. Johnson, A. J. Surman and L. Cronin, *J. Am. Chem. Soc.*, 2015, **137**, 5662.
48 X. X. Li, Y. X. Wang, R. H. Wang, C. Y. Cui, C. B. Tian and G. Y. Yang, *Angew. Chem., Int. Ed.*, 2016, **55**, 6462.
49 M. Z. Chi, H. J. Li, X. Xin, L. Qin, H. J. Lv and G. Y. Yang, *Inorg. Chem.*, 2022, **61**, 8467.
50 X. Du, Y. Ding, F. Song, B. Ma, J. Zhao and J. Song, *Chem. Commun.*, 2015, **51**, 13925.
51 H. L. Li, C. Lian and G. Y. Yang, *Inorg. Chem.*, 2021, **60**, 14622.
52 C. A. Chen and G. Y. Yang, *Inorg. Chem.*, 2023, **62**, 14163.
53 T. T. Cui, L. Qin, F. Y. Fu, X. Xin, H. J. Li, X. K. Fang and H. J. Lv, *Inorg. Chem.*, 2021, **60**, 4124.
54 Z. W. Wang, Q. Zhao, C. A. Chen, J. J. Sun, H. J. Lv and G. Y. Yang, *Inorg. Chem.*, 2022, **61**, 7477.
55 L. Jiao, Y. Y. Dong, X. Xin, L. Qin and H. J. Lv, *Appl. Catal., B*, 2021, **291**, 120091.
56 X. López, C. Bo and J. M. Poblet, *J. Am. Chem. Soc.*, 2002, **124**, 12574.